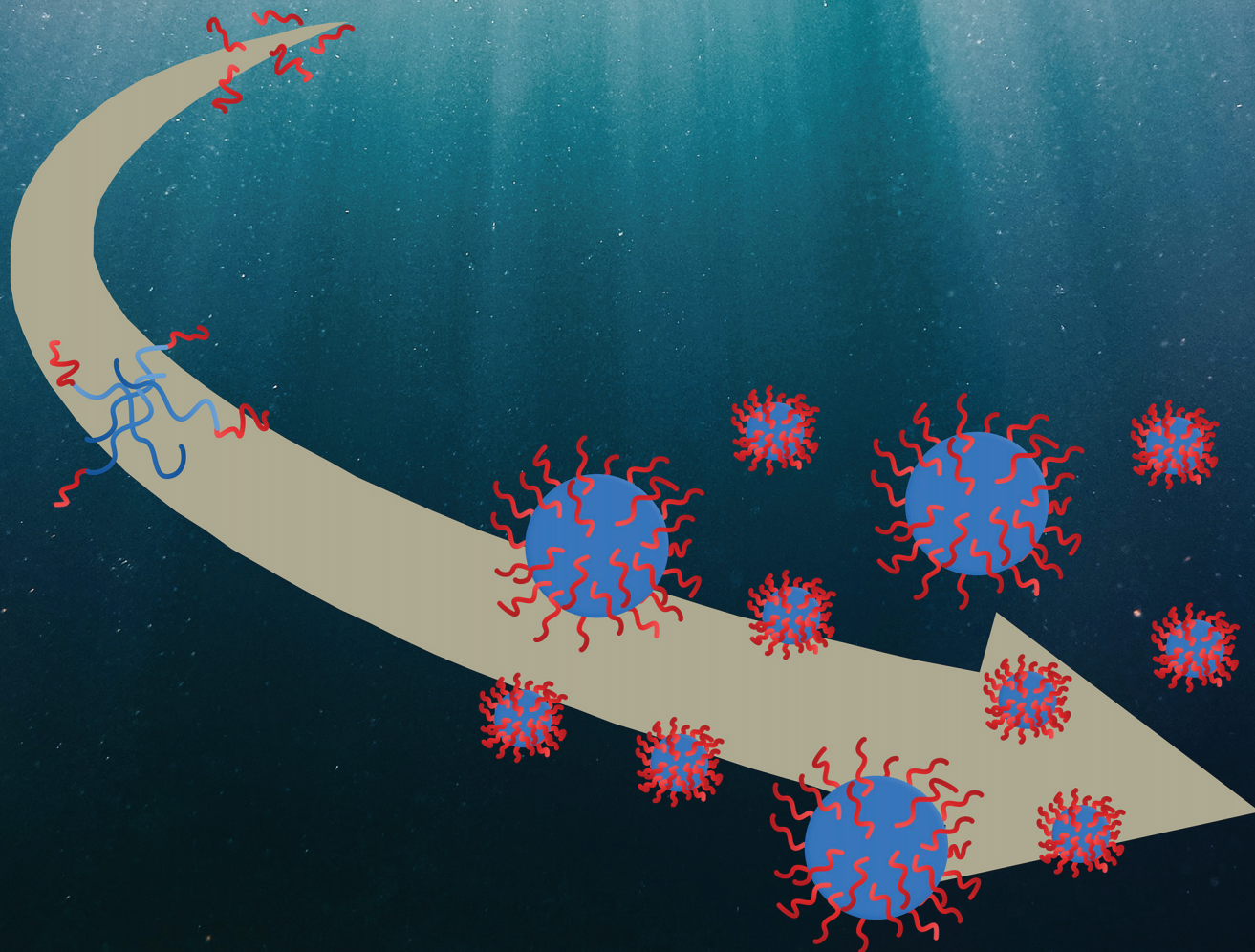


Polymer Chemistry

Volume 14
Number 19
21 May 2023
Pages 2259-2406

rsc.li/polymers



ISSN 1759-9962

PAPER

Eva Malmström *et al.*
Bimodal nanolatexes prepared *via* polymerization-induced
self-assembly: losing control in a controlled manner

PAPER

[View Article Online](#)
[View Journal](#) | [View Issue](#)

Cite this: *Polym. Chem.*, 2023, **14**, 2308

Bimodal nanolatexes prepared *via* polymerization-induced self-assembly: losing control in a controlled manner†

Alexandros E. Alexakis, ^{a,b} Olivia R. Wilson^a and Eva Malmström ^{*a,b}

The combination of reversible addition–fragmentation chain-transfer (RAFT) polymerization with polymerization-induced self-assembly (PISA) is known to yield monodisperse nanolatexes. Interestingly, based on the results of the current study, reproducible bimodal nanolatexes were shown to be the result of chain extension of protonated poly(2-dimethylaminoethyl methacrylate) (PDMAEMA) with methyl methacrylate (MMA) in water when aiming for a longer hydrophobic block, for which we provide the first imaging data to our knowledge. The bimodality was found to be induced by the hydrophilic Z-group of the RAFT agent, which has been reported in the literature to be the cause of bimodal molecular weight distributions in RAFT-mediated PISA in emulsion polymerization. Moreover, the advantages of such reproducible bimodal size distribution nanolatexes in coating applications were investigated briefly, underlining the possibilities of their one-pot synthesis. It was found that when bimodal nanolatexes are adsorbed onto cellulose filter paper, the contact angle against water is higher compared to chemically similar monomodal nanolatexes. Also, the morphological arrangement was found to be dependent on the drying protocol. This study aims to expand our understanding on bimodality and the identification of parameters that could promote it on demand to target high-end applications.

Received 27th January 2023,
Accepted 16th March 2023

DOI: 10.1039/d3py00090g

[rsc.li/polymers](#)

Introduction

In light of the increasing demand for functional nanoparticles that can be used in various applications, including paints and coatings, emulsion polymerization is widely used for their preparation.¹ Emulsion polymerization is an industrially well-established heterogeneous technique which enables the polymerization of hydrophobic monomers in water, thus exhibiting eco-friendly characteristics. However, in emulsion polymerization the stability of the hydrophobic polymer is achieved by low molecular weight surface active agents, called surfactants, which depending on the application might lead to their migration to surfaces.²

A way to tackle this shortcoming while maintaining the eco-friendly nature is through reversible addition–fragmentation chain-transfer (RAFT) polymerization. RAFT was first reported

in 1998³ and has since been a versatile polymerization technique giving access to complex polymeric architectures.⁴ In RAFT, a chain transfer agent, called the RAFT agent, usually a thiocarbonylthio or trithiocarbonate moiety, provides control over the molecular weight and polydispersity of the final polymer.^{3,5} There are two parameters that are of paramount importance in controlling the polymerization, both of which are related to the chemistry of the RAFT agent: the leaving group referred to as the R-group and the group that provides stability by controlling the reactivity of the C=S bond to the RAFT agent, referred to as the Z-group. In a recent case, the significance of the chemical composition of the RAFT agent was demonstrated, where a mixture of two RAFT agents was used to tune the molecular weight distribution and polydispersity index of polymers prepared by RAFT polymerization.⁶ There are numerous publications that have identified the ideal R- and Z-groups depending on the type of functional monomer that is to be polymerized. For instance, for methacrylates, trithiocarbonate-based RAFT agents, having a carboxylic acid as the R-group and an aliphatic chain for the Z-group, are ideal for controlling the molecular weight of the final polymers.^{5,7}

By combining RAFT with a technique called polymerization-induced self-assembly (PISA), the facile synthesis of nanoparticles can be achieved.^{8–12} During PISA, a hydrophilic

^aKTH Royal Institute of Technology, School of Engineering Sciences in Chemistry, Biotechnology and Health, Department of Fibre and Polymer Technology, Division of Coating Technology, Teknikringen 56-58, SE-100 44 Stockholm, Sweden.
E-mail: mavem@kth.se

^bWallenberg Wood Science Centre (WWSC), Teknikringen 56-58, SE-100 44 Stockholm, Sweden

† Electronic supplementary information (ESI) available. See DOI: <https://doi.org/10.1039/d3py00090g>



macromolecule (macroRAFT agent) is chain extended with a hydrophobic monomer in water, forming an amphiphilic diblock copolymer. At a certain ratio between the hydrophilic and hydrophobic blocks, self-stabilized nanoparticles are formed, which grow in size during polymerization.¹³ The RAFT-mediated PISA technique offers a versatile tool for the preparation of nanolatexes with properties such as size, charge density, a hydrophilic shell and hydrophobic core, which can be tailored on demand.^{14–19} Previously in our group, spherical cationic nanolatexes comprising a protonated poly(2-dimethylaminoethyl methacrylate) (PDMAEMA) shell and a poly(methyl methacrylate) (PMMA) core were synthesized *via* RAFT-mediated PISA and used for the tailored modification of cellulosic fibers.^{9,10,12} The RAFT agent (4-cyano-4-thiothiopropylsulfanyl pentanoic acid (CTPPA)) employed in polymerization had an aliphatic chain as the Z-group and a carboxylic acid as the R-group, which, as described previously, provided satisfying control over the final molecular weight, size, and polydispersity.

Nanolatexes comprising blocks with the same chemical composition were also synthesized by replacing the CTPPA RAFT agent with 4-(((2-carboxyethyl)thio)carbonothioyl)thio)-4-cyanopentanoic acid (CCCPA).^{20,21} In contrast to CTPPA, both the R- and Z-groups of CCCPA are composed of carboxylic acid units. Although monodisperse nanolatexes were prepared at a low DP of the hydrophobic PMMA core, surprisingly at higher DPs reproducible bimodal nanolatexes were obtained, which is the main topic of this study.

The advantageous impact of bimodal nanoparticles has been demonstrated in photonic, biosensor and anti-microbial applications due to their close packing.^{22–24} Hitherto, these bimodal nanoparticles are primarily formed by mixing monodisperse nanoparticles at predetermined ratios. However, having a process for preparing bimodal nanoparticles in one pot would be advantageous. In this work, we demonstrate the controlled and reproducible synthesis of bimodal nanolatexes prepared *via* RAFT-mediated PISA (Scheme 1) and we briefly explore the opportunities provided by the one-pot bimodal size distribution nanolatexes in coating applications.

Experimental

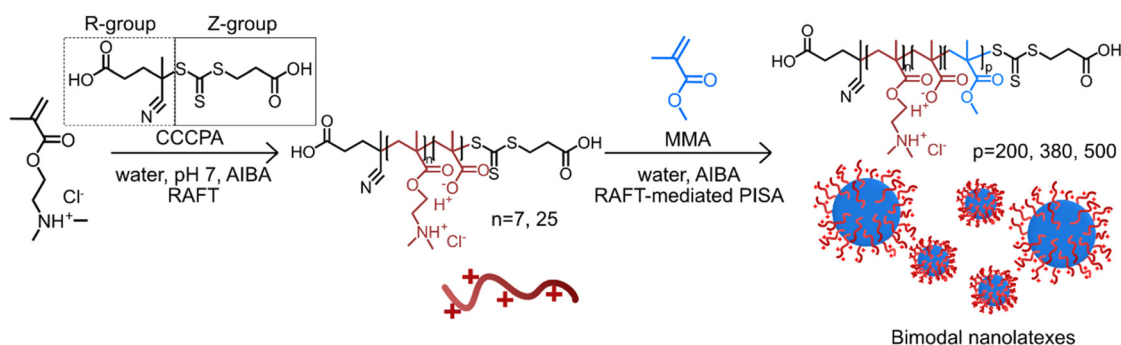
Materials

4-(((2-Carboxyethyl)thio)carbonothioyl)thio)-4-cyanopentanoic acid (CCCPA, 95%) was purchased from Boron Molecular and used as received. 2,2'-Azobis(2-methylpropionamide) dihydrochloride (AIBA, 97%), (2-dimethylaminoethyl) methacrylate (DMAEMA, 98%), methyl methacrylate (MMA, 99%) and tetrahydrofurfuryl methacrylate (THFMA, 97%) were purchased from Sigma-Aldrich and used as received. Hydrochloric acid (HCl, 37 wt%, AnalaR NORMAPUR®), deuterium oxide (D₂O, 99.9%) and dimethyl sulfoxide-d₆ (DMSO-d₆, 99.9%), were purchased from VWR. The water used was deionized or, when specified, Milli-Q (18.2 MΩ cm, Millipore Milli-Q Purification System). Dialysis tubing with MWCO of 1 kDa and 6–8 kDa (Spectra/Por® Biotech) were purchased from VWR. Silicon wafers were purchased from TOPSIL (RFQ of 150 mm/SZ/1-0-0/BORON/P type/Resis 4-6 Ohm/Thick 610-640/Oxy 27.1-33 MIXED/38647 + 52A0N31711E + D).

In this work, the nanolatexes were composed of a PDMAEMA shell (D) and a PMMA core (M) with varying degrees of polymerization (DPs) of both D, *i.e.* 7 or 25 referred to as D₇ and D₂₅, respectively and M, *i.e.* 200, 380 and 500, referred to as M₂₀₀, M₃₈₀ and M₅₀₀, respectively (Table 1). The preparation of the macroRAFT agents and their resulting nanolatexes was performed according to previous publications from our group and the amounts used for their synthesis are summarized in Table S1.^{†20,21} The same synthetic protocol was employed for the preparation of cationically charged nanolatexes with a PTHFMA (T) core, referred to as D₂₅-T₁₀₀, D₂₅-T₂₀₀ and D₂₅-T₃₀₀. More information regarding the kinetics of their polymerization and chemical composition can be found in the ESI (parts 1 to 5).[†]

Nuclear magnetic resonance (NMR)

The NMR spectra were recorded using a Bruker Avance 400 spectrometer (¹H: 400.13 MHz) equipped with a 5 mm broadband multinuclear (PABBO) probe at 25 °C using Bruker TopSpin v2.1 software. ¹H-NMR was used to follow the kinetics



Scheme 1 Schematic representation of the preparation of bimodal cationically charged nanolatexes *via* RAFT-mediated PISA. The charged hydrophilic macroRAFT agent is primarily composed of protonated PDMAEMA, which during polymerization is slightly hydrolyzed; thus, a tiny fraction of methacrylic acid (MAA) is present in the final macroRAFT agent.²⁰



Table 1 Physicochemical properties of the nanolatexes synthesized by RAFT-mediated PISA. The properties of the D₇ and D₂₅ macroRAFT agents are listed in Table S3†

Samples	Experimental DP _{MMA}	<i>M_n</i> ^a (g mol ⁻¹)	<i>D</i> _{large} ^b (nm)	<i>D</i> _{small} ^b (nm)	<i>D_H</i> ^c (nm)	PdI ^c	ζ ^c (mV)	<i>T_g</i> ^d (°C)
D ₇ -M ₂₀₀	172	18 700	80 ± 12	45 ± 10	89 ± 3	0.11 ± 0.02	62 ± 1	121 ± 1
D ₇ -M ₅₀₀	435	45 100	163 ± 12	67 ± 12	149 ± 3	0.16 ± 0.02	36 ± 1	122 ± 1
D ₂₅ -M ₃₈₀	323	36 600	78 ± 5	32 ± 4	112 ± 2	0.04 ± 0.01	56 ± 2	123 ± 3
D ₂₅ -M ₅₀₀	425	46 800	125 ± 12	62 ± 9	136 ± 2	0.03 ± 0.01	60 ± 1	125 ± 1

^a Molecular weight was calculated from eqn (S3).[†] ^b Diameter of the small (*D*_{small}) and large (*D*_{large}) nanolatexes measured by FE-SEM on spin-coated silica was evaluated using Gwyddion software. ^c Hydrodynamic diameter, polydispersity index and zeta potential measured by DLS with 0.1 wt% dispersion in deionized water. ^d Glass transition temperature obtained by DSC.

of the synthesized macroRAFT agents in D₂O (Fig. S2 and S3†). The data analysis was performed using MestReNova v14.2.0 software.

Differential scanning calorimetry (DSC)

A Mettler-Toledo DSC 1 instrument system was used to measure the glass transition temperature (*T_g*) of the freeze-dried nanolatexes. Measurements were performed under nitrogen flow (50 mL min⁻¹) from -20 to +200 °C with a heating/cooling rate of 10 °C min⁻¹. The heating/cooling protocol comprised of a heating ramp from 30 to 200 °C, stabilized at 200 °C for 5 min and then cooled down to -20 °C, followed by an isotherm for 5 min. Finally, the samples were heated from -20 to 200 °C and *T_g* was evaluated from them (Fig. S7†). The data were evaluated using Mettler Toledo STARe v. 15.00 software as per ISO standards.

Dynamic light scattering (DLS)

The hydrodynamic diameter (*D_H*), polydispersity index (PdI) and electrophoretic mobility (ζ) of the nanolatexes were determined using a Malvern Zetasizer NanoZS at 25 °C. Each value used in this study is averaged over 15 measurements and reported as the average over three consecutive runs. For all measurements, the concentration of the nanolatex dispersions was 0.1 wt% in deionized water. The standard used for the size correlation of the investigated latexes was polystyrene set by default from the software.

Size exclusion chromatography (THF-SEC)

SEC analysis was performed using a Waters system (Waters Sverige AB, Sollentuna, Sweden) using Empower software. The eluent used was THF and separation was performed using Waters Ultrastaygel (HR4, HR2, and HR0.5) solvent efficient analytical columns in series with a Styragel guard column (4.6 mm × 300 mm, thermostated at 35 °C). The system was coupled to a Waters-2998 photodiode-array detector (PDA), operated at 254 nm. Standard calibration was performed with polystyrene standards with molecular weights ranging from 176 kg mol⁻¹ to 266 g mol⁻¹ using data from the RI detector. All samples were dissolved in THF and filtered through a 0.45 μm polytetrafluoroethylene (PTFE) syringe filter. The results are shown in Fig. S4 and S5.†

Quartz crystal microbalance with dissipation (QCM-D)

The adsorbed amount and the viscoelastic properties of the adsorbed layer of nanolatexes on quartz crystals was determined by QCM-D (E4 model, Q-Sense AB, Gothenburg, Sweden). All experiments were conducted at pH 6 and ambient temperature with a nanolatex concentration of 0.025 g L⁻¹. The adsorption of nanolatexes took place after a stable baseline was achieved at a flow rate of 0.3 mL min⁻¹. The adsorption was monitored for 1 h with a 0.1 mL min⁻¹ flow rate and a final washing step with deionized water of 10 min. The adsorbed amount (*Γ*) was calculated using the Sauerbrey equation:²⁵

$$\Gamma = C(\Delta f/n), \quad (1)$$

where *C* is the sensitivity constant (-0.177 mg m⁻² Hz⁻¹), *n* is the overtone number (3 in this study) and Δ*f* is the change in frequency (Hz).

With QCM-D, the viscoelastic properties can also be studied through the dissipation factor of the adsorbed layer:

$$D = E_{\text{dissipated}}/(2\pi E_{\text{stored}}), \quad (2)$$

where *E*_{dissipated} is the dissipated energy of one oscillation period and *E*_{stored} is the stored energy in the oscillating system. Although the Sauerbrey equation is a model applied for rigid films, studies have shown that it is also valid for systems with higher dissipation compared to more advanced viscoelastic models.²⁶

Field emission scanning electron microscopy (FE-SEM)

A Hitachi S-4800 FE-SEM was used for imaging nanolatexes (KW-4A-2, Chemat Technology, Northridge, CA, USA). The voltage used was set at 1 kV for all images taken. Each sample was sputtered with Pt/Pd (Cressington sputter coater 208RH) for 10 s.

Contact angle (CA) measurement

The CA against water of the nanolatex-adsorbed QCM-D crystals both before and after annealing (Fig. S12†), the CA of the nanolatex-modified filter papers before and after annealing (Fig. S13†) and the CA of the nanolatex-modified silica wafers dried in the conditioning room and in an oven at 150 °C for 3 min (Fig. S15†) were monitored by using a Theta Lite optical tensiometer coupled with a remote-controlled syringe (Biolin



Scientific). All samples were kept at 50% RH at ambient temperature for at least 24 h before the measurement. The sessile drop method with a volume of 4 μL was used. Images were evaluated using OneAttention software (Biolin Scientific) to obtain the average contact angle (θ). Each sample was measured at three discrete positions.

Annealing of nanolatex-adsorbed crystals

All nanolatex-adsorbed QCM-D crystals were annealed in an oven at 150 $^{\circ}\text{C}$ for 5 h as described previously in the literature.^{8,20,21} Afterwards, the samples were left for at least 24 h (RH 50%) before characterizing them with the CA and by FE-SEM.

Results and discussion

This work focuses on the reproducible preparation of bimodal nanolatexes *via* the RAFT-mediated PISA technique and their subsequent film formation on substrates.

Cationically charged nanolatexes composed of a protonated PDMAEMA shell and a hydrophobic PMMA core were prepared *via* RAFT-mediated PISA (Scheme 1).^{20,21} The RAFT agent used in this study, 4-(((2-carboxyethyl)thio)carbonothioyl)thio-4-cyanopentanoic acid (CCCPA), comprising carboxylic acid groups in both the R- and the Z-groups, yielded high livingness of the macroRAFT agents (up to 97%, eqn (S1), ESI section 1†). In previous publications, nanolatexes of the same chemical composition, but with lower degrees of polymerization (DP) of MMA were monomodal and monodisperse as evaluated by dynamic light scattering (DLS) and field emission scanning electron microscopy (FE-SEM).^{20,21} However, CCCPA has been reported to result in bimodal molecular weight distributions and subsequent loss of control of polymerization during PISA.²⁷

Although no such observation was made for the molecular weight distribution in the aforementioned studies,^{20,21} in the current study, the bimodality was initially investigated *via* size exclusion chromatography (SEC) with THF as an eluent (Fig. S4 and S5†). The chromatograms exhibited clear bimodal characteristics, *i.e.* splitting of the peak or appearance of a shoulder;²⁷ however, the molecular weight values obtained were significantly higher than the theoretical results, Table 1. This could be due to three reasons: (i) the values obtained were outside the linear region of columns, (ii) the charged block of the copolymer may interact with the SEC columns, and (iii) according to the DLS investigation in THF (Table S4†), some aggregation was observed, possibly indicating incomplete molecular solubility. However, according to ^1H -NMR performed in THF- d_8 , characteristic polymers peaks could be identified (Fig. S5†).

Irrespective of the bimodality observed by THF-SEC, DLS analysis yielded monomodal nanolatex characteristics in water. In particular, the hydrodynamic diameter (D_{H}) of the nanolatexes seemed to be monodisperse according to the polydispersity index (PDI) and their cationic characteristic was veri-

fied by a positive zeta potential (ζ) (Table 1). For the evaluation of D_{H} by DLS, a spherical morphology is assumed by default by the instrument. FE-SEM was used to image dried spin-coated nanolatex dispersions on silica to complement the observations obtained from DLS (Fig. 1). Although the spherical morphology was corroborated, a bimodal size distribution was observed for all nanolatexes. Based on the FE-SEM images, the diameters of the small (D_{small}) and the large (D_{large}) nanolatexes were measured as listed in Table 1. The values for D_{large} were similar to D_{H} , indicating the low sensitivity of DLS towards the small nanolatexes. This is due to the relationship between the nanoparticle size and the wavelength of the incident light in DLS, where large nanoparticles have a greater impact on D_{H} , meaning that smaller nanoparticles appear invisible to the instrument.^{8,28,29}

A possible explanation for the observed difference between D_{small} and D_{large} (Table 1) could be the ratio between the hydrophilic and hydrophobic blocks. For instance, in the cases of $D_{7\text{-M}_{500}}$ and $D_{25\text{-M}_{500}}$, $\text{DP}_{\text{hydrophilic}}/\text{DP}_{\text{hydrophobic}}$ is 0.02 and 0.06, respectively, when the actual DPs determined gravimetrically are considered (Table 1). Since the advantage of PISA relies on varying this ratio in order to achieve complex morphological architectures, this three-fold difference is expected to have a significant influence on nanolatex morphology.

Recently, in a work of Zetterlund *et al.*,²⁷ the preparation of nanolatexes with bimodal molecular weight distributions *via* RAFT-mediated PISA in emulsion polymerization using multiple RAFT agents, including CCCPA, was reported.

According to their study, monomer-swollen hydrophobic domains are created by macroRAFT agents and a few monomer units, which ideally act as nucleating sites to form amphiphilic diblock copolymers and, at higher monomer conversions, nanolatexes. It was explained that during the fragmentation of the macroRAFT agent, a short hydrophilic moiety containing the Z-group, the hydrophobic oligomer and the decomposed initiator will exit this hydrophobic domain ("Z-group induced RAFT exit"). This will consequently lead to fewer but larger nanolatexes in the final dispersion, and as a result, loss of control over polymerization as stoichiometry becomes compromised. The Z-group induced RAFT exit occurred only when the Z-group of the RAFT agent was hydrophilic. A similar RAFT agent to CCCPA, which contained a Z-group with an aliphatic chain instead of a carboxylic acid, 4-cyano-4-thiothiopropylsulfanyl pentanoic acid (CTPPA), was previously demonstrated to successfully stabilize monomodal PDMAEMA-shelled and PMMA-cored nanolatexes, further supporting this claim.^{9,10,12} Consequently, the absence of the carboxylic acid prevented the formation of bimodal nanolatexes. Hence, in the present study, the Z-group induced RAFT exit is hypothesized to be the reason for the bimodal size distributions imaged to our knowledge for the first time. Additionally, the fact that, in the current work, P(DMAEMA-*b*-MMA) nanolatexes exhibited bimodal characteristics similar to those reported in the work of Zetterlund *et al.*, where the nanolatexes were composed of poly(methacrylic acid-*b*-styrene),



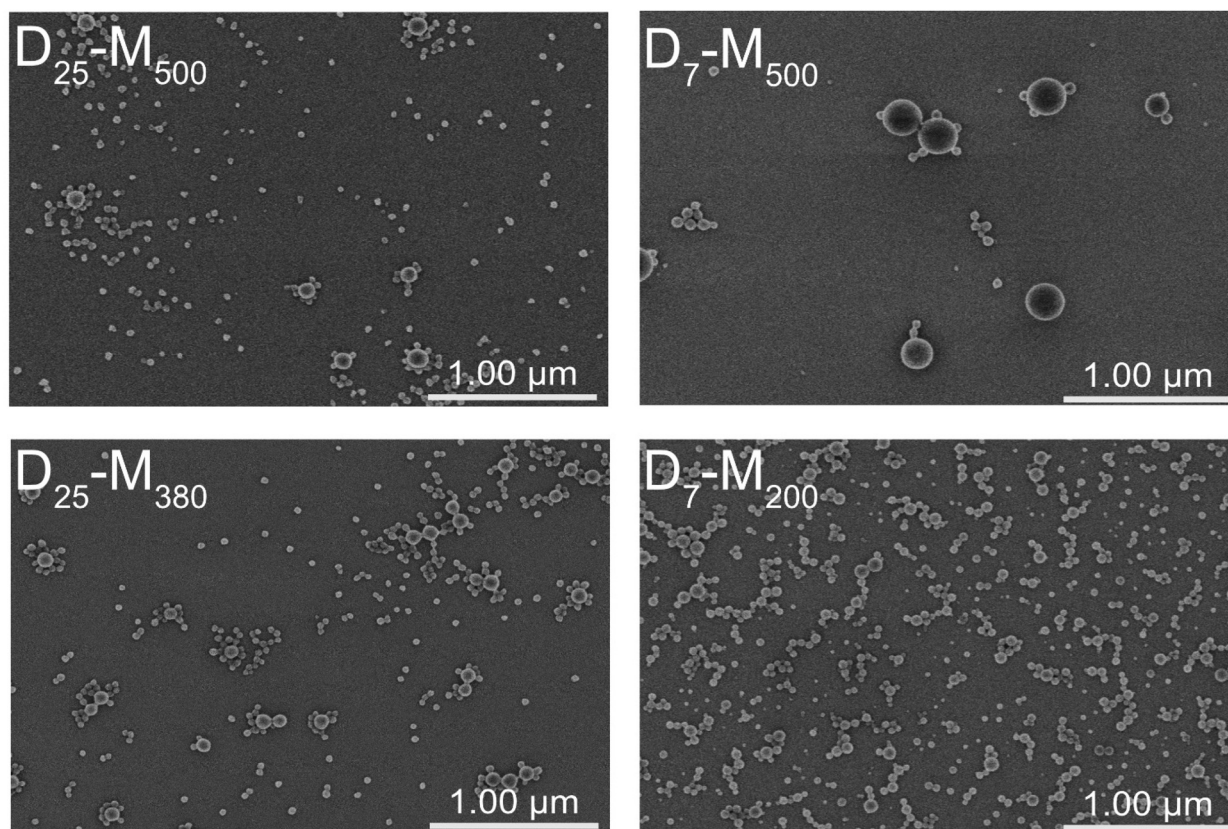


Fig. 1 FE-SEM of the spin-coated bimodal nanolatexes. The scale bar in all FE-SEM images is 1 μm .

indicates that this process is not only characteristic of a specific hydrophilic–hydrophobic combination.

The syntheses of the $D_{25}\text{-}M_{380}$ and $D_{25}\text{-}M_{500}$ nanolatexes were repeated three times, and the resulting D_{small} , D_{large} and D_{H} for each batch were similar when considering the MMA conversion (Table S5 and Fig. S8†). This clearly indicates the reproducibility of the bimodal size distributions derived from the Z-group induced RAFT exit.

As a case study, $D_{25}\text{-}M_{500}$ was selected to investigate in detail the morphological evolution during RAFT-mediated PISA. According to FE-SEM imaging, bimodal nanolatexes can be seen already after 15 min (Fig. 2). Additionally, D_{large} , D_{small} and D_{H} were plotted against the polymerization time (Fig. 2). All of the different diameter values follow an increasing trend, reaching a plateau after 60 min, which coincides with the final MMA conversion achieved for this system. Based on the Z-group induced RAFT exit, we hypothesize that the escaping moieties aggregate into new hydrophobic domains and that the chain extension proceeds there, which is supported by the increasing trend observed for D_{small} .

In order to verify that bimodal nanolatexes result from the Z-group induced RAFT exit and in extension from the hydrophilic Z-group of the RAFT-agent irrespectively of the core-polymer, tetrahydrofurfuryl methacrylate (THFMA) was polymerized *via* RAFT-mediated PISA using the D_{25} macroRAFT agent (Table S2†). The FE-SEM images revealed that bimodal

nanolatexes are formed when DP_{THFMA} was 300 (Fig. S9†). In the case of PMMA-cored nanolatexes, the diameter after which bimodal nanolatexes was observed was approximately 80 nm, which in the case of THFMA was 180 nm. This could be an additional reason why bimodal nanolatexes were not obtained in our previous studies, as higher DP of MMA, and thus size, have to be reached.^{20,21} Additionally, the water solubility of the hydrophobic monomer, *i.e.*, 15 g L^{−1} (ref. 30) and 1.8 g L^{−1} (ref. 31) for MMA and THFMA, respectively, its chemical structure, and the pH of the emulsion (protonated or deprotonated carboxylic acid groups of the RAFT agent) could affect the escaping process and are considered potential parameters for tuning the Z-group induced RAFT exit on demand.

Film formation properties of bimodal nanolatexes

In this section, we report the film formation of the aforementioned one-pot bimodal nanolatexes and their surface properties, thus highlighting the opportunities of the controlled bimodality originating from the Z-group induced RAFT exit.

The adsorption of bimodal nanolatexes was first investigated by quartz crystal microbalance with dissipation (QCM-D). Nanolatex dispersions of 0.025 g L^{−1} were adsorbed onto QCM-D (silica) crystals and their adsorption was compared to known monodisperse nanolatexes of the same chemical composition, *i.e.*, PDMAEMA-shell and PMMA-core (Fig. 3, $D_{7}\text{-}M_{100}$, $D_{25}\text{-}M_{200}$).²⁰ Although small differences with regard



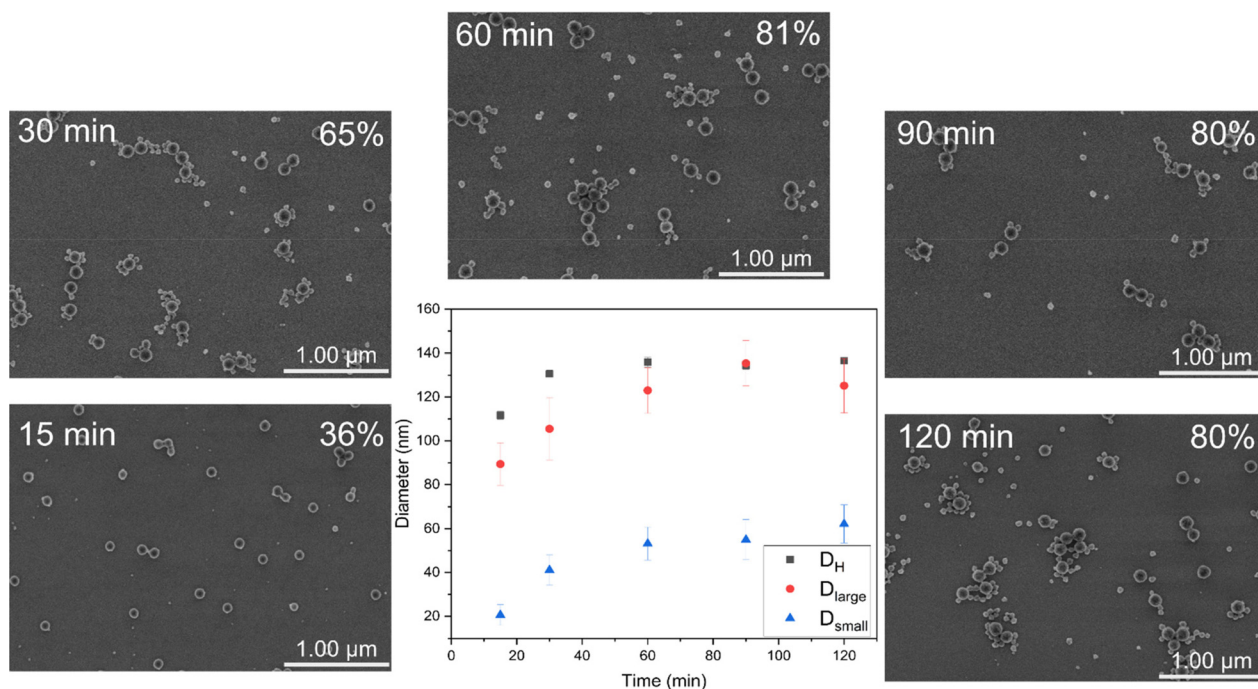


Fig. 2 FE-SEM of the spin-coated D_{25} - M_{500} during the polymerization time. In the middle graph, their respective diameters obtained from FE-SEM compared to the ones obtained from DLS are shown. The MMA conversion is shown on the top right corner of each FE-SEM image and the scale bar for all images is 1 μ m.

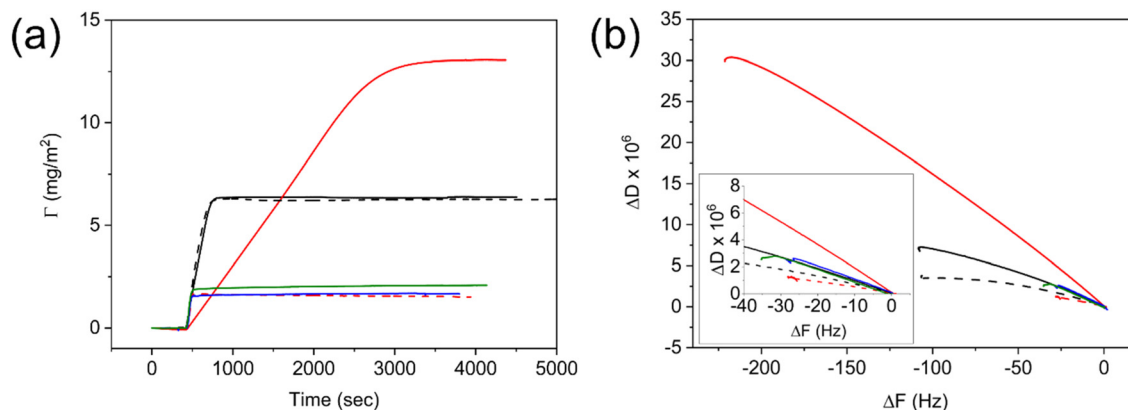


Fig. 3 Adsorbed amount (a) and dissipation of the nanolatexes against the frequency (b) obtained from QCM-D; monomodal nanolatexes: D_7 - M_{100} (black dashed line) and D_{25} - M_{200} (red dashed line) and bimodal nanolatexes: D_7 - M_{500} (black line), D_7 - M_{500} (red line), D_{25} - M_{380} (blue line) and D_{25} - M_{500} (green line).

to the adsorbed amount (Γ , Fig. 3a) and dissipation (ΔD , Fig. S10†) can be seen between the monomodal and bimodal nanolatexes, the adsorption mechanism seems to be very different for the case of the bimodal D_7 - M_{500} .

An extended slope with a lower incline was observed for D_7 - M_{500} , whereas for every other nanolatex used, both the incline and the slope were similar. This is due to the bimodal adsorption mechanism, which is primarily affected by the adsorption of heavier nanolatexes, and it is clearly depicted in Fig. 3b, where the change in dissipation was plotted against the change in frequency.³² The arrangement resulting from their

adsorption was imaged by FE-SEM (Fig. S11†). It was observed that an effective, repulsive, area around each nanolatex is created dependent on the charge density as formerly observed.²⁰

Previously, it has been reported that, when nanolatexes with a PDMAEMA-shell are adsorbed onto different substrates, they can be annealed above T_g to create a homogeneous polymeric coating.^{8,20,21} In this study, we verify this observation by subjecting the nanolatex-modified substrates previously used in QCM-D to an annealing protocol involving heating to 150 $^{\circ}$ C for 5 h as per previous publications.^{8,20,21} The corres-



ponding morphologies were imaged by FE-SEM (Fig. S11†). The annealed nanolatexes were characterized by an increased diameter as formerly described.²⁰ Additionally, the contact angles (CAs) against water of the nanolatex-modified substrates prior to and after annealing were monitored (Fig. S12†). Prior to annealing, the adsorption of cationically charged nanolatexes reduced the CA since they reduced the hydrophobicity of the substrate, whereas after annealing, the PMMA-core of the nanolatexes was exposed as a consequence of rearrangement, thus increasing the CA against water.

In order to demonstrate the advantages of bimodal over monomodal nanolatexes in film formation, two experiments were conducted: (i) bimodal nanolatexes were adsorbed onto cellulose filter papers and their morphology and CA before and after annealing were investigated and (ii) bimodal nanolatex dispersions were drop-casted onto silica wafers and dried

either in a conditioning room at 23 °C and 50% RH or in an oven at 150 °C for 3 min. These two drying protocols were used to investigate the influence of the drying procedure on the final arrangement of the nanolatexes on the silica wafers.

Bimodal nanolatex-modified cellulose filter papers were imaged by FE-SEM prior to and after annealing at 150 °C for 5 h (Fig. 4). The CA after annealing for bimodal nanolatex-modified cellulose filter papers reached 120° compared to approximately 100° obtained from monomodal nanolatex-modified cellulose filter papers with the same PDMAEMA-shell.⁸ This is possibly due to the closer packing in the case of the bimodal nanolatexes.

In a second experiment, involving adsorption onto silica, the drying mechanism seemed to be different for the two investigated drying procedures (Fig. 5 and S14†). In particular, when the concentration of the nanolatex dispersion was

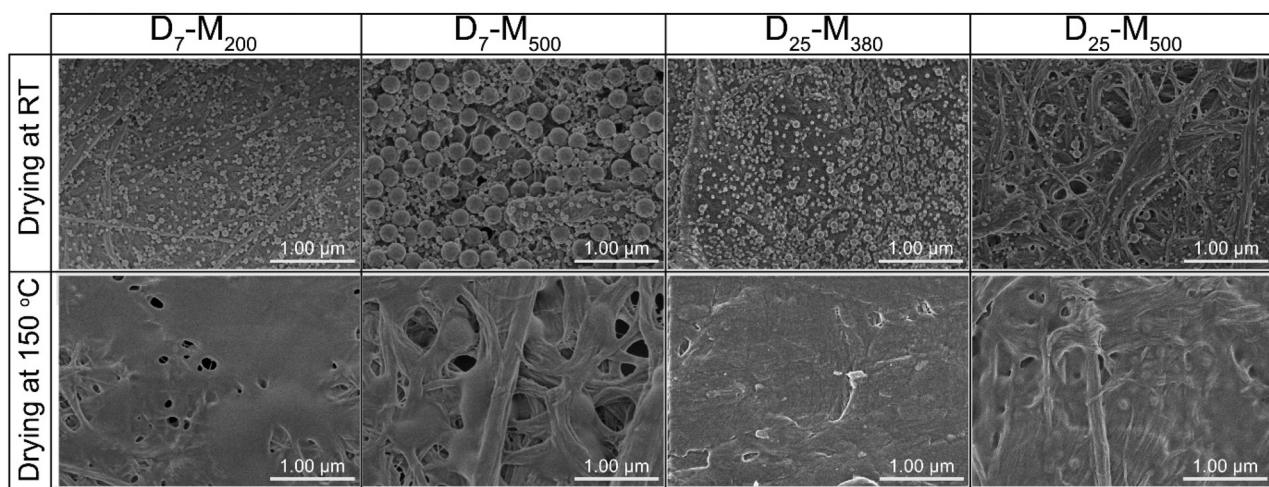


Fig. 4 FE-SEM of the nanolatex-modified filter papers before (top) and after (bottom) annealing at 150 °C for 5 h. The scale bar in all images is 1 μm.

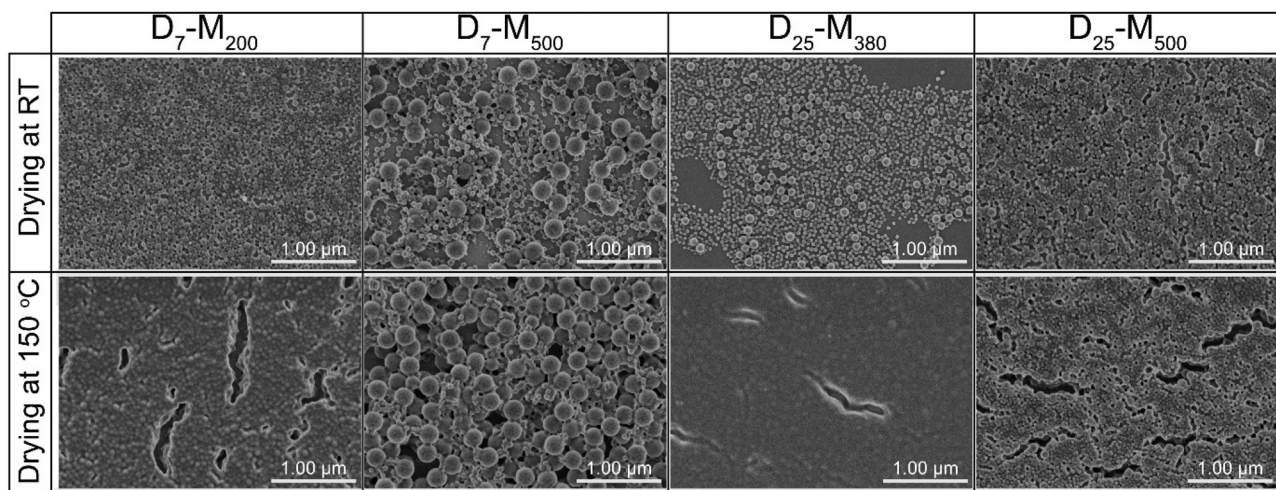


Fig. 5 FE-SEM of the nanolatexes (0.1 wt%) dried in the conditioning room (top) or in an oven (bottom) at 150 °C for 3 min. The scale bar in all images is 1 μm.



0.1 wt%, D₇-M₂₀₀ and D₂₅-M₅₀₀ exhibited mixed drying mechanisms, where large and small nanolatexes were homogeneously mixed when dried (Fig. 5). However, in the cases of D₇-M₅₀₀ and D₂₅-M₃₈₀, the drying mechanism seemed to follow a “large-on-top” arrangement, which was more apparent when drying was performed under mild conditions in the conditioning room compared to the forced approach used with the oven-drying protocol. A similar arrangement was also observed for the cases of D₇-M₅₀₀ and D₂₅-M₃₈₀ when adsorbed onto cellulose filter paper (Fig. 4, top) prior to annealing. According to the literature, the different drying mechanisms of bimodal colloidal nanoparticles are derived from their different Peclet numbers (Pe), which originate from their different diffusion rates.²² For instance, the case of the “large-on-top” drying mechanism can be expected when the Pe for the large (Pe_{large}) and small (Pe_{small}) nanolatexes are higher and lower than 1, respectively.³³ This means that the diffusion rate of the large nanolatexes is higher than the drying rate of the dispersion and the opposite for the small nanolatexes. In all drying experiments, regardless of the drying protocol used, the silica wafers became iridescent (see graphical abstract), which is direct evidence of nanolatex morphological arrangement on the surface, previously reported for other binary colloidal crystals.²³

Conclusions

In this work, we have presented the first microscopy images to our knowledge of bimodal nanolatexes prepared *via* RAFT-mediated PISA in emulsion polymerization. This bimodality was found to be driven by the hydrophilicity of the Z-group of the RAFT agent, a notion that has been reported as “Z-group induced RAFT exit”.

Moreover, we provided FE-SEM images following the evolution of the resulting bimodal nanolatexes. Our findings suggest that bimodality is reproducible when using CCCPA, where the water solubility, the chemical structure of the hydrophobic monomer and its DP are amongst the key parameters for tuning it on demand.

We also compared the adsorption of the mono- and bimodal nanolatexes on silica by QCM-D and found that higher adsorbed amounts were achieved for the latter. Moreover, the film formation properties of the bimodal nanolatexes on cellulose filter paper and silica wafers were studied. It was found that closer packing of the nanolatexes increased the contact angle (CA) against water due to the more homogeneous hydrophobic coating layer after annealing, compared to the monomodal nanolatex-modified cellulose filter papers present in the literature, where lower CAs were obtained. In addition, the drying process seemed to influence the final packing arrangement (governed by the Pe) of the nanolatex on the silica wafers. Furthermore, these substrates became opal-like and iridescent due to the morphological arrangement of the bimodal nanolatexes.

We envision that the results of this study will enhance the possibilities of using RAFT-mediated PISA to prepare controlled bimodal nanolatexes in one pot with tailored properties by exploiting the bimodality as an advantageous modification platform.

Author contributions

Alexandros E. Alexakis: conceptualization, data curation, formal analysis, investigation, methodology, validation, visualization, and writing – original draft. Olivia R. Wilson: validation and writing – review and editing. Eva Malmström: funding acquisition, project administration, resources, supervision, and writing – review and editing.

Conflicts of interest

There are no conflicts to declare.

Acknowledgements

The authors acknowledge funding from the Knut and Alice Wallenberg Foundation (KAW) through the Wallenberg Wood Science Centre.

References

- 1 R. Lambourne and T. A. Strivens, *Paint and surface coatings: theory and practice*, 2nd edn, 1999.
- 2 S. C. Thickett and R. G. Gilbert, *Polymer*, 2007, **48**, 6965–6991.
- 3 J. Chiefari, Y. K. Chong, F. Ercole, J. Krstina, J. Jeffery, T. P. T. Le, R. T. A. Mayadunne, G. F. Meijs, C. L. Moad, G. Moad, E. Rizzardo and S. H. Thang, *Macromolecules*, 1998, **31**, 5559–5562.
- 4 A. Gregory and M. H. Stenzel, *Prog. Polym. Sci.*, 2012, **37**, 38–105.
- 5 D. J. Keddie, *Chem. Soc. Rev.*, 2014, **43**, 496–505.
- 6 R. Whitfield, K. Parkatzidis, N. P. Truong, T. Junkers and A. Anastasaki, *Chem*, 2020, **6**, 1340–1352.
- 7 S. Perrier, *Macromolecules*, 2017, **50**, 7433–7447.
- 8 A. E. Alexakis, J. Engström, A. Stamm, A. V. Riazanova, C. J. Brett, S. V. Roth, P. O. Syren, L. Fogelström, M. S. Reid and E. Malmström, *Green Chem.*, 2021, **23**, 2113–2122.
- 9 J. Engström, C. J. Brett, V. Körstgens, P. Müller-Buschbaum, W. Ohm, E. Malmström and S. V. Roth, *Adv. Funct. Mater.*, 2020, **30**, 2070098.
- 10 J. Engström, F. L. Hatton, L. Wågberg, F. D’Agosto, M. Lansalot, E. Malmström and A. Carlmark, *Polym. Chem.*, 2017, **8**, 1061–1073.
- 11 P. B. Zetterlund, S. C. Thickett, S. Perrier, E. Bourgeat-Lami and M. Lansalot, *Chem. Rev.*, 2015, **115**, 9745–9800.



- 12 L. Carlsson, A. Fall, I. Chaduc, L. Wågberg, B. Charleux, E. Malmström, F. D'Agosto, M. Lansalot and A. Carlmark, *Polym. Chem.*, 2014, **5**, 6076–6086.
- 13 C. J. Ferguson, R. J. Hughes, D. Nguyen, B. T. T. Pham, R. G. Gilbert, A. K. Serelis, C. H. Such and B. S. Hawkett, *Macromolecules*, 2005, **38**, 2191–2204.
- 14 S. Varlas, T. J. Neal and S. P. Armes, *Chem. Sci.*, 2022, **13**, 7295–7303.
- 15 N. J. W. Penfold, J. Yeow, C. Boyer and S. P. Armes, *ACS Macro Lett.*, 2019, **8**, 1029–1054.
- 16 E. E. Brotherton, F. L. Hatton, A. A. Cockram, M. J. Derry, A. Czajka, E. J. Cornel, P. D. Topham, O. O. Mykhaylyk and S. P. Armes, *J. Am. Chem. Soc.*, 2019, **141**, 13664–13675.
- 17 M. J. Derry, L. A. Fielding and S. P. Armes, *Prog. Polym. Sci.*, 2016, **52**, 1–18.
- 18 S. Sugihara, A. Blanazs, S. P. Armes, A. J. Ryan and A. L. Lewis, *J. Am. Chem. Soc.*, 2011, **133**, 15707–15713.
- 19 A. Blanazs, S. P. Armes and A. J. Ryan, *Macromol. Rapid Commun.*, 2009, **30**, 267–277.
- 20 A. E. Alexakis, M. R. Telaretti Leggieri, L. Wågberg, E. Malmström and T. Benselfelt, *J. Colloid Interface Sci.*, 2023, **634**, 610–620.
- 21 A. E. Alexakis, Å. Jerlhagen, M. R. T. Leggieri, A. Eliasson, T. Benselfelt and E. Malmström, *Macromol. Chem. Phys.*, 2023, **224**, 2200249.
- 22 B. S. He, I. Martin-Fabiani, R. Roth, G. I. Toth and A. J. Archer, *Langmuir*, 2021, **37**, 1399–1409.
- 23 F. S. Diba, A. Boden, H. Thissen, M. Bhawe, P. Kingshott and P. Y. Wang, *Adv. Colloid Interface Sci.*, 2018, **261**, 102–127.
- 24 Z. F. Dai, Y. Li, G. T. Duan, L. C. Jia and W. P. Cai, *ACS Nano*, 2012, **6**, 6706–6716.
- 25 Z. P. G. Sauerbrey, *Z. Phys.*, 1959, **155**, 206–222.
- 26 C. Aulin, I. Varga, P. M. Claesson, L. Wågberg and T. Lindström, *Langmuir*, 2008, **24**, 2509–2518.
- 27 T. R. Guimaraes, Y. L. Bong, S. W. Thompson, G. Moad, S. Perrier and P. B. Zetterlund, *Polym. Chem.*, 2021, **12**, 122–133.
- 28 S. Bhattacharjee, *J. Controlled Release*, 2016, **235**, 337–351.
- 29 C. M. Hoo, N. Starostin, P. West and M. L. Mecartney, *J. Nanopart. Res.*, 2008, **10**, 89–96.
- 30 National Center for Biotechnology Information. PubChem Compound Summary for CID 6658, 2022.
- 31 National Center for Biotechnology Information. PubChem Compound Summary for CID 17151, 2022.
- 32 A. L. J. Olsson, I. R. Quevedo, D. Q. He, M. Basnet and N. Tufenkji, *ACS Nano*, 2013, **7**, 7833–7843.
- 33 R. E. Trueman, E. Lago Domingues, S. N. Emmett, M. W. Murray and A. F. Routh, *J. Colloid Interface Sci.*, 2012, **377**, 207–212.

